

SHENGHU LUO ¹, TONG WANG ^{2*}, YONGPING WU ²,
JINGYU HUANGFU ², HUATAO ZHAO ³

INTERNAL MECHANISM OF ASYMMETRIC DEFORMATION AND FAILURE CHARACTERISTICS OF THE ROOF FOR LONGWALL MINING OF A STEEPLY DIPPING COAL SEAM

Stability control of the roof is the key to safe and efficient mining of the longwall working face for a steeply dipping coal seam. In this study, a comprehensive analysis was performed on the roof destruction, migration, and filling characteristics of a steeply dipping longwall working face in an actual coalmine. Elastic foundation theory was used to construct a roof mechanics model; the effect of the coal seam inclination angle on the asymmetric deformation and failure of the roof under the constraint of an unbalanced gangue filling was considered. According to the model, increasing the coal seam angle, thickness of the immediate roof, and length of the working face as well as decreasing the thickness of the coal seam can increase the length of the contact area formed by the caving gangue in the lower area of the slope. Changes to the length of the contact area affect the forces and boundary conditions of the main roof. Increasing the coal seam angle reduces the deformation of the main roof, and the position of peak deflection migrates from the middle of the working face to the upper middle. Meanwhile, the position of the peak rotation angle migrates from the lower area of the working face to the upper area. The peak bending moment decreases continuously, and its position migrates from the headgate T-junction to the tailgate T-junction and then the middle of the working face. Field test results verified the rationality of the mechanics model. These findings reveal the effect of the inclination coal seam angle on roof deformation and failure and provide theoretical guidance for engineering practice.

Keywords: steeply dipping seam, gangue, slip filling, deformation failure, main roof, angle effect

¹ XI'AN UNIVERSITY OF SCIENCE AND TECHNOLOGY, DEPARTMENT OF MECHANICS, CHINA

² XI'AN UNIVERSITY OF SCIENCE AND TECHNOLOGY, SCHOOL OF ENERGY ENGINEERING, CHINA

³ SHANDONG MINING MACHINERY GROUP CO., LTD. CHINA

* Corresponding author: 670298140@qq.com



© 2021. The Author(s). This is an open-access article distributed under the terms of the Creative Commons Attribution-NonCommercial License (CC BY-NC 4.0, <https://creativecommons.org/licenses/by-nc/4.0/deed.en>) which permits the use, redistribution of the material in any medium or format, transforming and building upon the material, provided that the article is properly cited, the use is noncommercial, and no modifications or adaptations are made.

1. Introduction

A steeply dipping coal seam is understood to have a buried angle of 35° - 55° ; such coal seams are difficult to mine [1,2]. The key to the safe and efficient mining of steeply dipping coal seams is stability control of the roof-support-floor system, which is affected by the behavior of the surrounding strata [3,4].

The coal-forming environment of steeply dipping coal seams is complicated, and such seams are extremely difficult to safely and efficiently mine. In the 1970s, the Soviet Union developed fully mechanized mining technologies for mining thick, medium-thick, and steeply dipping coal seams [5,6]. In the 1980s and 1990s, the United States, Germany, France, United Kingdom, India, Spain, and other countries also explored mechanized mining methods and ground control techniques for accessing steeply dipping coal seams and used these to carry out limited experimental mining [7]. After nearly two decades of research and development, China has made significant progress in developing the mining theory, technology applications, and equipment needed to mine steeply dipping coal seams, successfully achieved a transformation from non-mechanized mining to fully mechanized longwall mining (fully mechanized caving) under certain conditions, and solved the basic safety problem of mining in steeply dipping seams. However, with the exception of some mines in which the fully mechanized mining of medium-thick coal seams or the fully mechanized caving of some extra-thick coal seams takes place, mines are in general still using non-mechanized mining methods such as oblique short-wall and longwall mining. In such mines, low production and efficiency, poor safety and operating environments, and frequent casualty-inducing accidents remain important factors restricting production and operation.

A core issue for longwall mining of a steeply dipping coal seam is the deformation and migration characteristics of the main roof, which control the surrounding rock of the working face. A steeply dipping coal seam will cause the gangue to slide down the gob during the mining process [8]. Uneven filling of the gob can cause the roof to collapse, and the surrounding strata show obvious asymmetric behavior [9]. Many approaches have been used to study the stress distribution of the roof for different mining processes of steeply dipping coal seams, deformation and failure laws of the roof [10-15], failure mode and evolution process of the main roof [16-19], and influence of gangue on strata behavior [20-23]. The above research has improved understanding of the relationship between roof deformation and strata behavior, which has laid the foundation for further research on steeply dipping coal seams. The coal seam angle is known to affect asymmetric deformation and failure of the roof [24]. Determining the behavioral response of the roof for the longwall working face of a steeply dipping coal seam under unbalanced load and constraint conditions is very important for understanding the law of strata behavior and guiding onsite practice [25]. Further study is urgently needed to quantitatively characterize the slip of the gangue filling from the immediate roof based on the coal seam angle, the mechanical structure and characteristics of roof movement under the constraint of gangue filling, and other internal mechanisms.

This study focused on the steeply dipping working face of an actual coalmine as the research target. First, a similar material experiment was performed to study the deformation, failure, and slip characteristics of the roof. Second, elastic foundation theory was used to construct a roof mechanics model, which was used to study the effect of the coal seam angle on the asymmetric deformation and failure of the roof under the constraint of unbalanced gangue filling. Finally, field monitoring was performed to analyze the localized load characteristics and dispersion de-

gree of the supports, and the results were used to verify the rationality of the model. This study provides a theoretical reference for the law of strata behavior governing the longwall mining face of steeply dipping coal seams.

2. Background

Working face 25221 of coalmine 2130 (Xinjiang Coking Coal Group Ewirgol) is located in district 2 of the #5 coal seam. The working face is located west of ditch #15 ditch and 153 m east of line 16. The surface is mountainous and filled with gullies. The working face has a long and narrow distribution from east to west. The mining elevation is +2047-2120 m, the strike length is 2098 m, and the inclined length is 100 m. The angle fluctuates within 36°-46° with an average of 45°. The coal bulk density is 1.35 t/m³. The coal seam is stable with a thickness of 3.58-9.77 m and average thickness of 5.77 m. The hardness coefficient f of the coal is 0.3-0.5. The spontaneous combustion tendency is $\Delta T = 9-14^{\circ}\text{C}$; this is less than 20°C, which indicates grade IV coal. The explosiveness index of the coal dust is $V_r = 24\%-45\%$; this is in the range of 0.1-1.0, which indicates medium explosiveness. The gas emission volume is 1.52-4.62 m³/t, which indicates an abnormal gas mine. The coal and rock characteristics of the working face are presented in Table 1.

TABLE 1

Characteristics of coal and rock strata

Layer	Rock	Thickness (m)	Characteristics
Main roof	Medium sandstone	17	Rock is dominated by quartz, which has strong resistance to weathering, and well-developed bedding surfaces.
Immediate roof	Gravelly coarse sandstone	2.32	Rock is off-white; mud is cemented, weathered, and fragile.
Coal seam	#5 coal	3.58-7.0	Contains 3-5 layers of gangue; height of interbedded gangue is 1.4-2.5 m.
Immediate floor	Carbon mudstone	17.06	Rock is off-white with mineral cement.
Main floor	Coarse sandstone	9.0	Rock joints are developed, weathered, and fragile.

3. Model test

3.1. Process and methods

A similarity simulation is a method for studying the laws of nature based on the similarities between things or phenomena. To understand the migration law of the surrounding rock and the support load distribution during mining, the geological conditions of coalmine 2130 were adopted. A 1500 mm × 1500 mm × 600 mm combined model frame independently designed and developed by Xi'an University of Science and Technology was selected. This three-dimensional experimental model can not only impose constraints in both the horizontal and vertical directions but also simulate short advances of the working face along the strike direction. A coal and rock

layer histogram was used to reduce the coalmine to an experimental model with a geometric similarity ratio of 1:20. The physical and mechanical parameters of the coal and rock mass measured onsite were used to determine the proportions of similar materials: 70-140 mesh quartz sand, coal ash, gypsum, and calcium carbonate. Water was added, and the materials were mixed evenly and placed in the model frame. A heavy object was used to compact the material to the required density. To represent the layers, 8-20 mesh mica powder was used. According to the law of similarity, the stress and strength similarity constant was 32, the time similarity constant was $20^{1/2}$, the bulk density similarity constant was 1.6, and the load similarity constant was 12800. A specially made support was used to conduct the experiment. High-precision sensors were installed in the leg, top, shield, and base of the support to monitor the vertical and lateral loads. A 108-channel pressure data acquisition system was used for data collection.

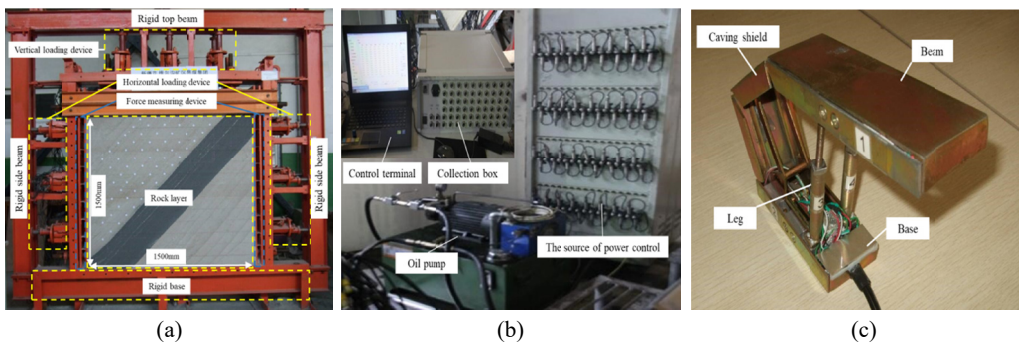


Fig. 1. Test model and device: (a) test model, (b) data collection system, and (c) support model

3.2. Results and analysis

The experimental results were as follows:

- (1) As the working face was inclined, gangue fell from the immediate roof into the gob. The gangue in the lower area of the gob was in small pieces; the filling was dense with high strength is greater. The gangue was in larger pieces in the middle and upper areas of the gob; the filling was loose and low in strength. The working face can be divided into a contact area where the filling body contacts the overlying strata and a noncontact area where it is not. The inclined profile of the filling body comprised a rectangle combined with a triangle, and it formed a hollow face on the upper area.
- (2) When the support advanced forward, large areas of the main roof and overlying strata caved in, and irregular stepped fractures formed along the strike and inclined directions (Figs. 2(c) and (d)). The gob in the middle area of the slope was half-filled; the rock mass was relatively loose, and the overlying strata had sufficient space for migration. The overhanging, rotating, fracturing, and caving processes were clearly observed. The gob in the upper area of the slope was mostly unfilled, and the overlying strata showed frequent breaks. The support may have suffered an impact that adversely affected the stability of the support-surrounding rock system. In particular, gas easily accumulated in the upper corner, which would significantly affect the safety of the working face.

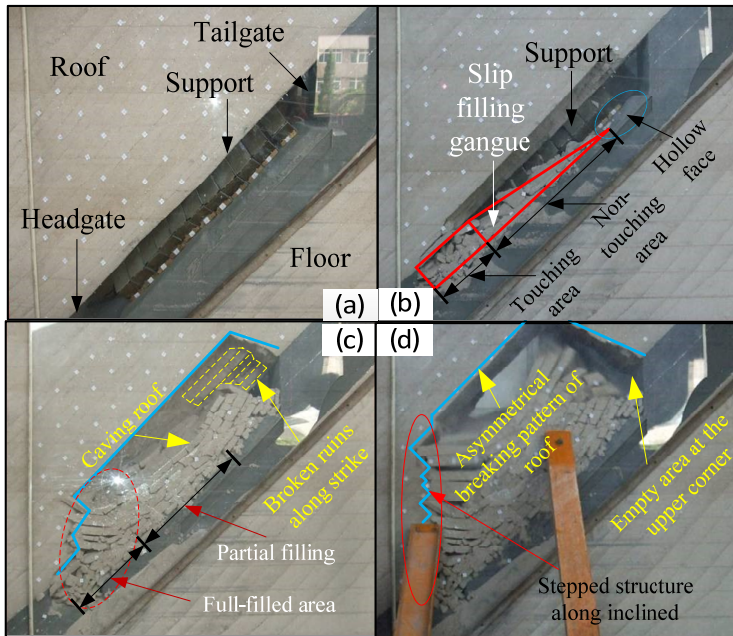


Fig. 2. Caving and filling characteristics of gangue

- (3) The working resistance of the support showed obvious localized distribution characteristics. The working resistance of the support was largest in the middle area. In the lower area, after the caving gangue slid down, a coal-support-gangue support structure formed along the strike. Then, the roof formed a voussoir beam structure. The presence of the large structure provided some support to the overlying strata (Fig. 3). Therefore,

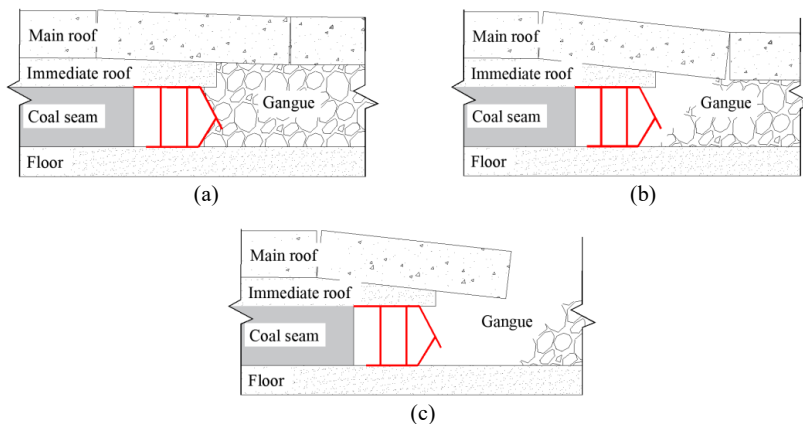


Fig. 3. Relationships of the support-surrounding rock system along the strike: (a) lower area, (b) middle area, and (c) upper area of the inclination

the support had the lowest working resistance at about 70.06% of that in the middle area. In the middle area, the immediate roof caved in and the main roof was part of the voussoir beam structure. Thus, the most bending and sinking of the roof took place here, and the largest load was acting on the support. In the upper area, a coal-support system formed along the strike. The gangue was far from the support, and the exposed length of the roof was small. The support was the main body bearing the weight of the roof. Therefore, the working resistance of the support was about 86.55% that of the middle area, which is about 86.55%.

For steeply dipping coal seams, the deformation and failure characteristics of the surrounding rock and gangue show obvious asymmetry. Increasing the coal seam angle gradually increases the non-uniformity of the gangue filling the gob, and the non-equilibrium constraints on the roof or floor become more obvious.

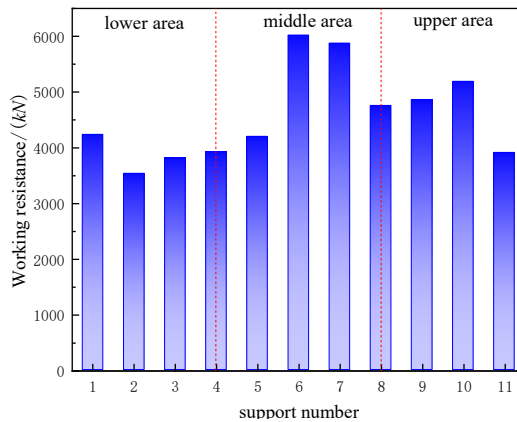


Fig. 4. Working resistance of supports

4. Slip of the gangue filling from the immediate roof

4.1. Analysis of the characteristics

The coal seam angle is the main factor that affects the slip characteristics of the gangue filling. The thickness and length of the immediate roof determine the volume of the caving gangue, and the thickness of the coal seam and inclined length of the working face determine the size of the movement space for the gangue. Fig. 5 shows the model established to characterize effects of the above factors on the gangue filling. The thickness of the coal seam is h_1 (m). The thickness of the immediate roof is h_2 (m). The inclined length of the contact area is a (m). The length of the working face is L (m). The coal seam angle is α ($^\circ$). The angle between the noncontact area of the filling body and horizontal direction is β ($^\circ$). The angle between the upper surface of the noncontact area of the filling body and the vertical direction is θ ($^\circ$), where $\theta = \frac{\pi}{2} - \alpha + \beta$. The expansion coefficient of the immediate roof is k .

Fig. 5 shows the characteristics of the gangue filling in the gob depending on the coal seam angle when the immediate roof is thin and the amount of caving gangue is small. The following relationship should be satisfied:

$$kh_2L \cdot 1 \leq \frac{1}{2}L(h_1 + h_2) \cdot 1 \quad (1)$$

When α is less than α_1 and slightly greater than the natural angle of repose, some of the gangue slides towards the lower area of the gob, but there is no filled area. The inclined profile of the filling body is triangular, as shown in Figs. 5(a) and (b). This results in the maximum exposed length of the main roof, and the deformation and failure characteristics are unrelated with the gangue. As the coal seam angle is increased, the form shown in Fig. 5(c) appears. When α is greater than α_1 , more gangue slides down, and the lower area of the gob is fully filled. The inclined profile of the filling body combines a rectangle and triangle. In the lower area, the contact area changes the force constraints and boundary conditions of the immediate roof, which affects its deformation and failure.

For the critical angle α_1 in Fig. 5(a), the following geometric relationship holds:

$$\tan \theta = \frac{BC}{h_1 + h_2} \quad (2)$$

The following filling relationship holds:

$$kh_2L \cdot 1 = \frac{1}{2}(h_1 + h_2)BC \cdot 1 \quad (3)$$

By incorporating Eq. (3) in Eq. (2), the critical angle α_1 can be obtained:

$$\alpha_1 = \frac{\pi}{2} + \beta - \arctan \frac{2kh_2L}{(h_1 + h_2)^2} \quad (4)$$

The filling relationship in Fig. 5(b) is

$$kh_2L \cdot 1 = \frac{1}{2}(h_1 + h_2)L \cdot 1 \quad (5)$$

This can be reorganized to obtain

$$h_2 = \frac{h_1}{2k - 1} \quad (6)$$

When the expansion coefficient of the caving gangue and the thicknesses of the immediate roof and coal seam meet the relationship described in Eq. (6) and the critical angle α_0 is achieved, then the inclination profile of the filling body is triangular, and the volume of the filling body is at its maximum.

For the gangue filling in Fig. 5(c), the following geometric relationship holds:

$$kLh_2 \cdot 1 = \left[a(h_1 + h_2) + \frac{1}{2}(h_1 + h_2)^2 \tan \theta \right] \cdot 1 \quad (7)$$

This can be reorganized to obtain the inclined length a of the contact area in Fig. 5(c):

$$a = \frac{kLh_2}{(h_1 + h_2)} - \frac{1}{2}(h_1 + h_2) \tan \theta \quad (8)$$

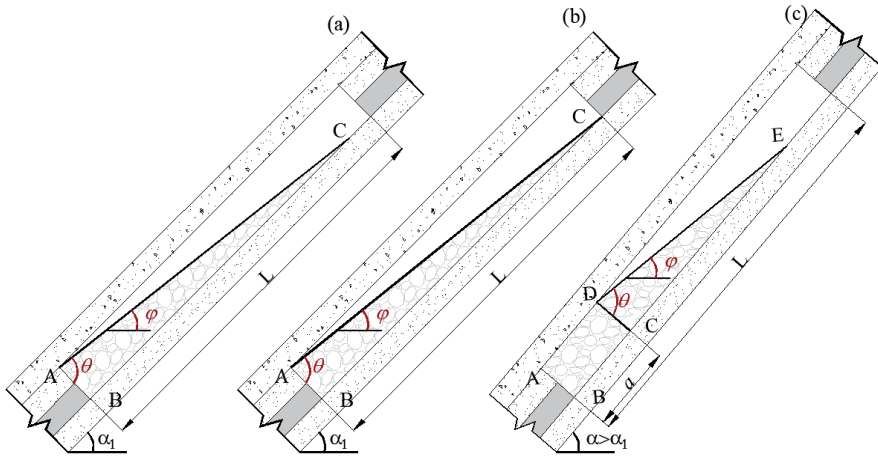


Fig. 5. Characteristics of gangue filling when the immediate roof is thin and the amount of caving gangue is small

Fig. 6 shows the characteristics of gangue filling the gob when the immediate roof is thick and amount of caving gangue is large. The following relationship should be satisfied:

$$kh_2L \cdot 1 > \frac{1}{2}L(h_1 + h_2) \cdot 1 \quad (9)$$

When α is less than α_1 and slightly greater than the natural angle of repose, a small amount of gangue will slide towards the lower area of the gob. The inclined profile of the filling body is shaped like a trapezium. The main roof is completely exposed, and the rock beam is easy to break, as shown in Fig. 6(a). When $\alpha_1 < \alpha < \alpha_2$, some gangue slides down, and a contact area appears in the lower area of the gob. The main roof is in full contact with the accumulated gangue, and the exposed length is reduced. The inclined profile of the filling body combines a rectangle and trapezoid. The accumulation of gangue changes the force constraint at the lower area of the main roof, and the caving gangue begins to affect the deformation and failure of the main roof, as shown in Fig. 6(b). When $\alpha_2 < \alpha$, the gangue does not stay in place after caving. The length of the contact area is further increased in the lower area of the gob. The gangue seriously affects the deformation and failure of the main roof, and the inclination profile of the filling body combines a rectangle and triangle, as shown in Fig. 6(d).

For the critical angle α_1 in Fig. 6(a), the following filling relationship holds:

$$kLh_2 \cdot 1 = \frac{L}{2}(h_1 + h_2 + CD) \cdot 1 \quad (10)$$

This is based on the following geometric relationship:

$$CD = (h_1 + h_2) - \frac{L}{\tan \theta} \quad (11)$$

Eq. (11) can be incorporated into Eq. (10) to obtain the critical angle α_1 :

$$\alpha_1 = \frac{\pi}{2} + \varphi - \arctan \frac{L}{2[(h_1 + h_2) - kh_2]} \quad (12)$$

When $\alpha_1 < \alpha < \alpha_2$, the following filling relationship holds:

$$kLh_2 = \left[L \cdot EF + a(h_1 + h_2 - EF) + \frac{1}{2} \tan \theta (h_1 + h_2 - EF)^2 \right] \cdot 1 \quad (13)$$

The following geometric relationship holds:

$$(h_1 + h_2) \tan \theta = L + EF \tan \theta - a \quad (14)$$

Then, Eqs. (13) and (14) can be combined to obtain the inclination length a of the contact area in Fig. 6(b):

$$a = L - \sqrt{2L \tan \theta (h_1 + h_2 - kh_2)} \quad (15)$$

For the critical angle α_2 in Fig. 6(c), the following filling relationship holds:

$$kLh_2 \cdot 1 = \left[a(h_1 + h_2) + \frac{1}{2}(L - a)(h_1 + h_2) \right] \cdot 1 \quad (16)$$

The following geometric relationship holds:

$$\tan \theta = \frac{L - a}{h_1 + h_2} \quad (17)$$

Eq. (17) can be incorporated into Eq. (16) to obtain the critical angle α_2 :

$$\alpha_2 = \frac{\pi}{2} + \varphi - \arctan \left[\frac{2L}{h_1 + h_2} - \frac{2kLh_2}{(h_1 + h_2)^2} \right] \quad (18)$$

When $\alpha_2 < \alpha$, the gangue accumulation pattern in Fig. 6(d) is the same as that in Fig. 5(c), and the length a of the contact area can be calculated with Eq. (8).

Thus, depending on the coal seam angle, the slip volume of the gangue filling and size of its migration space should be determined according to Eqs. (1) and (9). Then, the changes in the filling characteristics with the coal seam angle can be analyzed.

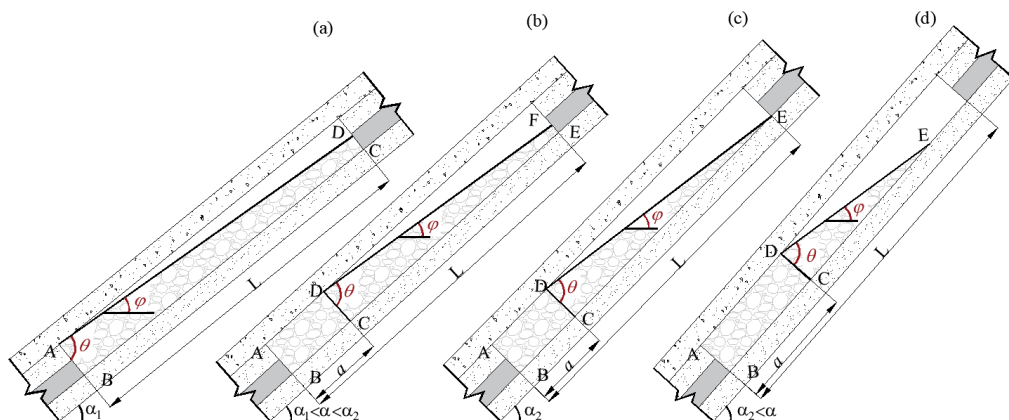


Fig. 6. Characteristics of gangue filling when the immediate roof is thick and amount of caving gangue is large

4.2. Analysis of influencing factors

The influences of the coal seam angle, thickness of the coal seam, thickness of the immediate roof, and inclined length of the working face on the characteristics of the gangue filling were analyzed. Fig. 7 shows the variations in the inclined length a of the contact area as the above factors were changed. The following results were obtained:

- (1) The inclined length a of the contact area increases logarithmically as the coal seam angle increases. When the coal seam angle is less than the natural angle of repose, the gangue

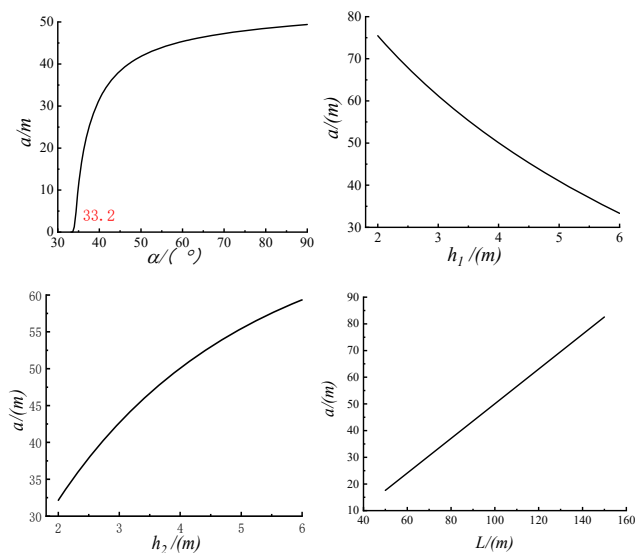


Fig. 7. Inclined length a of the contact area and the relationship between influencing factors

the mechanics model of the main roof, where the unit thickness is along the strike. The z -axis is vertical to the coal seam, and the x -axis is inclined upward along the working face. α is the coal seam angle ($^\circ$). j is the natural angle of repose of the gangue ($^\circ$). a is the inclined length of the contact area (m). L is the length of the working face (m). k_1 is the foundation coefficient of the coal and rock mass on both sides of the tailgate and headgate (kN/m^3). k_2 is the foundation coefficient of the gangue filling body in the gob (kN/m^3). $p(x)$ is the load of the overlying strata on the main roof and can be simplified as a linear function:

$$p(x) = p_0 - x\gamma \sin \alpha \cdot 1 \quad (19)$$

where p_0 is the load at section O (kN/m) and g is the weight (kN/m^3). The load $p(x)$ can be decomposed into the vertical rock beam load $p(x)\cos \alpha$ and parallel rock beam load $p(x)\sin \alpha$. In this study, only the effect of the vertical load on the main roof was considered, so $q(x) = p(x)\cos \alpha$.

5.1. Beam in the lower area

Fig. 9(a) shows the rock beam on the left side of section O. According to elastic foundation theory, the flexural differential equation is

$$\frac{d^4 z_1(x)}{dx^4} + 4\beta_1^4 z_1(x) = \frac{q(x)}{EI} \quad (20)$$

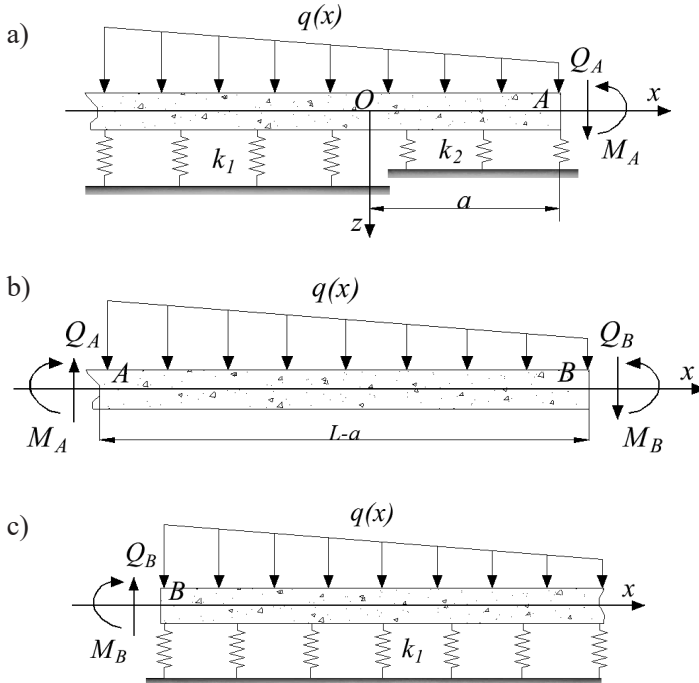


Fig. 9. Stress analysis of the main roof: beam in the (a) lower area, (b) middle area, and (c) upper area

where $\beta_1 = (k_1/EI)^{1/4}$ is a constant (m^{-1}), E is the elastic modulus (MPa), and I is the moment of inertia (m^4). The general solution to Eq. (20) is

$$z_1(x) = e^{\beta_1 x} (A_1 \cos \beta_1 x + B_1 \sin \beta_1 x) + e^{-\beta_1 x} (C_1 \cos \beta_1 x + D_1 \sin \beta_1 x) + \frac{q(x)}{k_1} \quad (21)$$

where $A_1, B_1, C_1,$ and D_1 are unknown constants. When x tends to $-\infty$, the deflection $z_1(x)$ of the beam tends to be constant; thus, $C_1 = D_1 = 0$. Eq. (21) can be simplified as

$$z_1(x) = e^{\beta_1 x} (A_1 \cos \beta_1 x + B_1 \sin \beta_1 x) + \frac{q(x)}{k_1} \quad (22)$$

5.2. Rock beam in the contact area

The contact area of the rock beam is section OA in Fig. 9(a). According to elastic foundation theory, the flexural differential equation is

$$\frac{d^4 z_2(x)}{dx^4} + 4\beta_2^4 z_2(x) = \frac{q(x)}{EI} \quad (23)$$

where $\beta_2 = (k_1/EI)^{1/4}$ is a constant (m^{-1}). The general solution to Eq. (23) is

$$z_2(x) = e^{\beta_2 x} (A_2 \cos \beta_2 x + B_2 \sin \beta_2 x) + e^{-\beta_2 x} (C_2 \cos \beta_2 x + D_2 \sin \beta_2 x) + \frac{q(x)}{k_2} \quad (24)$$

where $A_2, B_2, C_2,$ and D_2 are unknown constants.

5.3. Rock beam in the noncontact area

The rock beam in the noncontact area is shown in Fig. 9(b). M_A and M_B are the bending moments at sections A and B , respectively. Their relationship can be expressed as

$$M_B = M_A + Q_A(L-a) - \int_a^L q(x)(L-x) dx \quad (25)$$

Q_A and Q_B are the shear forces at sections A and B , respectively. Their relationship can be expressed as

$$Q_B = Q_A - \int_a^L q(x) dx \quad (26)$$

The flexural differential equation of the rock beam in the noncontact area is given by

$$\frac{d^2 z_3(x)}{dx^2} = -\frac{M_A}{EI} - \frac{Q_A}{EI}(x-a) + \frac{1}{EI} \int_a^x q(\xi)(x-\xi) d\xi \quad (27)$$

Integrating Eq. (27) twice obtains

$$z_3(x) = A_3 + B_3x + \frac{x^2}{120EI} \left[60M_A + 20a^3k_0 + 20aq_0x + 20(x-3a)Q_A + \right. \\ \left. + x^2(k_0x - 5q_0) - 10a^2(k_0x + 3q_0) \right] \quad (28)$$

where $k_0 = \sin \alpha \cdot \gamma \cdot \cos \alpha$, A_3 , and B_3 are unknown constants.

5.4. Beam in the upper area

The beam in the upper area is shown in Fig. 9(c). According to elastic foundation theory, the flexural differential equation is

$$\frac{d^4 z_4(x)}{dx^4} + 4\beta_1^4 z_4(x) = \frac{q(x)}{EI} \quad (29)$$

The general solution to Eq. (29) is

$$z_4(x) = e^{\beta_1 x} (A_4 \cos \beta_1 x + B_4 \sin \beta_1 x) + \\ + e^{-\beta_1 x} (C_4 \cos \beta_1 x + D_4 \sin \beta_1 x) + \frac{q(x)}{k_1} \quad (30)$$

where A_4 , B_4 , C_4 , and D_4 are unknown constants. When x tends to ∞ , the deflection $z_4(x)$ of the beam tends to be constant, so $A_4 = B_4 = 0$. Eq. (30) can be simplified as

$$z_4(x) = e^{-\beta_1 x} (C_4 \cos \beta_1 x + D_4 \sin \beta_1 x) + \frac{q(x)}{k_1} \quad (31)$$

According to the boundary conditions of section A, the following also holds:

$$-EIz_4''(b) = M_B, \quad -EIz_4'''(b) = Q_B \quad (32)$$

Then, the unknown constants C_4 and D_4 can be expressed as

$$C_4 = \frac{2\beta_1 e^{L\beta_1}}{k_1} [Q_B \cos L\beta_1 + \beta M_B (\cos L\beta_1 + \sin L\beta_1)] \\ D_4 = \frac{2\beta_1 e^{L\beta_1}}{k_1} [\beta_1 M_B (\cos L\beta_1 - \sin L\beta_1) - Q_B \cos L\beta_1]$$

5.5. Condition of continuity

In the above derivation process, A_1 , B_1 , A_2 , B_2 , C_2 , D_2 , A_3 , B_3 , M_A , and Q_A are still unknown constants. If the condition of continuity is assumed for the mechanics model shown in Figs. 8 and 9, then the values of the above unknown parameters can be determined. According to the condition of continuity at section O,

$$\begin{aligned} z_1(0) &= z_2(0), \quad z_1'(0) = z_2'(0), \\ z_1''(0) &= z_2''(0), \quad z_1'''(0) = z_2'''(0) \end{aligned} \quad (33)$$

According to the condition of continuity at section A,

$$\begin{aligned} z_2(a) &= z_3(a), \quad -EIz_2''(a) = M_A, \\ z_2'(a) &= z_3'(a), \quad -EIz_2'''(a) = Q_A \end{aligned} \quad (34)$$

According to the condition of continuity at section B,

$$z_3(L) = z_4(L), \quad z_3'(L) = z_4'(L) \quad (35)$$

Eqs. (33)-(35) can be combined with the rock beam deflections given by Eqs. (22), (24), (28), and (31) to determine the deformation law of the main roof under different loading and constraint conditions. These equations can also be used to determine the deflection, bending moment, and shear force of the rock beam.

6. Example

To study the law of deformation and failure for the roof of a steeply dipping coal seam, the mechanics model was applied to working face 25221 of coalmine 2130. The length of the working face was 100 m, the natural angle of repose of the gangue was 30° , the foundation coefficient of the coal rock mass was 1000 kN/m^3 , the foundation coefficient of the gangue was 300 kN/m^3 , and the elastic modulus of the main roof was $8.0 \times 10^4 \text{ MPa}$. The values of the parameters were selected by combining engineering examples and values reported in related research.

Fig. 10 shows the deflection and rotation of the rock beam according to the coal seam angle. The following can be observed:

- (1) As the coal seam angle increased, the peak deflection of the main roof gradually decreased. The central axis of the peak deflection shifted in the upper area (i.e., the rate of reduction and shift gradually increased), and the slight deformation at both ends gradually decreased. The peak rotation gradually decreased, and its position shifted from the headgate to the tailgate.
- (2) When the coal seam angle was less than the natural angle of repose of the gangue, the peak deflection of the main roof was at the middle of the working face, and the peak rotation was at the lower area of the working face. Both ends were slightly deformed. At coal seam angles of 20° , 25° , and 30° , the peak deflections were 0.32979, 0.30269, and 0.27512 m at 49.2, 49.3, and 49.5 m, respectively, from the headgate. The peak rotations were 0.008265, 0.007615, and 0.00695 rad at 14.3, 14.5, and 14.7 m, respectively. Because the coal seam angle was less than the natural angle of repose of the gangue, the gangue stayed in place after caving. A noncontact area occurred at the lower area of the working face. The overhang length of the main roof was at its maximum, and the peak deflection was relatively large. However, as the coal seam angle increased, the normal component of the stress from the rock layer's self-weight decreased. The positions of the peak deflection and rotation shifted slightly, and the deflection and rotation of the rock beam decreased accordingly. Increasing the coal seam angle from

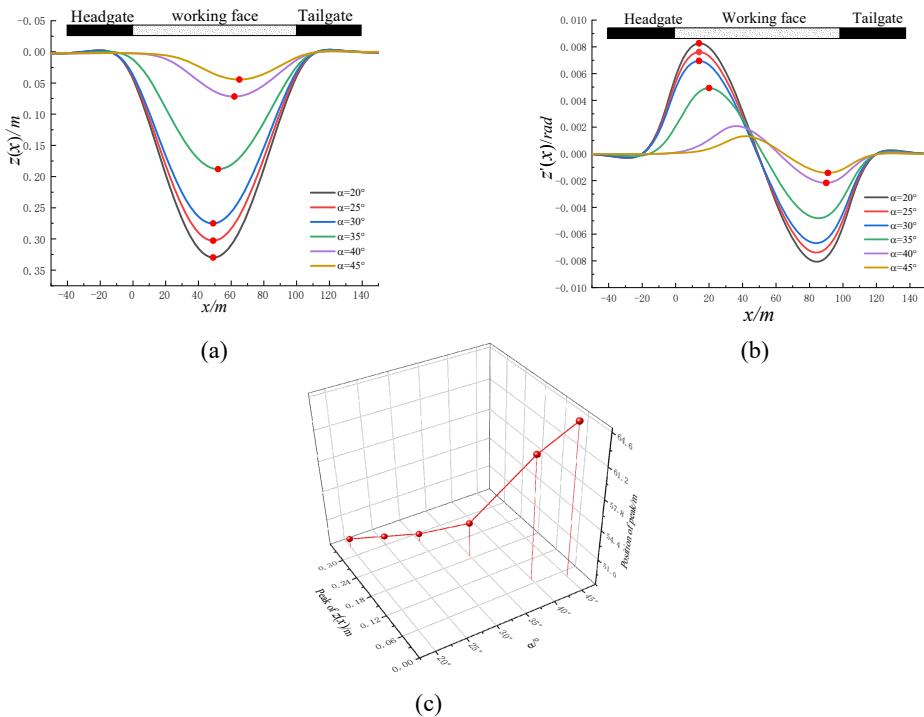


Fig. 10. Deflection and rotation diagram of the rock beam at different angles: (a) deflection, (b) rotation, and (c) deflection varies with angle

20° to 25° and 30° reduced the deflection by 8.2% and 16.58%, respectively, and the rotation by 7.86% and 15.91%, respectively.

- (3) When the coal seam angle was greater than the natural angle of repose of the gangue, the position for the peak deflection of the main roof shifted to the upper area of the working face. The position of the peak rotation shifted from the headgate to the tailgate, and the deformation at both ends of the working face decreased. At coal seam angles of 35°, 40°, and 45°, the peak deflections were 0.188, 0.07176, and 0.0444 m at positions of 52, 62, and 65 m, respectively. The peak rotations were 0.00492, -0.00216, and -0.00142 rad at positions of 21, 90, and 91 m, respectively. When the coal seam angle was greater than the natural angle of repose, the gangue could not stay in place and slid or rolled downwards along the working face. The accumulation of caving gangue formed a contact area ($a = 11.4, 31.58, \text{ and } 38.37 \text{ m}$) at the lower area of the working face, which changed the boundary constraints of the main roof. The overhang length of the main roof decreased, and the normal component of the stress from the rock layer's self-weight also decreased. Reducing the coal seam angle from 35° to 40° and 45° decreased the deflection by 61.8% and 76.38%, respectively, and the rotation by 56.01% and 71.12%, respectively. Therefore, when the coal seam angle was greater than the natural angle of repose, the slip of the gangue filling has a greater impact on the roof deformation, and the deformation of the surrounding rock was greatly reduced.

Fig. 11 shows the bending moment and shear of the rock beam at different angles. The following can be observed:

- (1) When the coal seam angle was small, the peak bending moments were slightly larger at the headgate and tailgate than at the middle of the working face. As the coal seam angle was increased, the peak bending moment of the main roof gradually decreased. The peak central axis of the middle area shifted upward, the peak central axis of the headgate shifted slightly upward, and the peak central axis of the tailgate shifted slightly downward. The reduction rate and shift of the peak gradually increased with the coal seam angle. The position of the peak shear force continuously shifted upward from the headgate as the coal seam angle increased, and the change in length was closely related with the length of contact area.
- (2) When the coal seam angle was less than the natural angle of repose, the peak bending moments were slightly larger at the headgate and tailgate than at the middle area of the working face. When the coal seam angles were 20° , 25° , and 30° , the peak bending moments were -1416.16 , -1309.3 , and -1199.23 kN-m at positions of -3.1 , -3.2 , and -3.25 m, respectively. The peak shear forces were 104.496 , 97.837 , and 90.785 kN, respectively; all were at the position of 0 m. The deformation and failure characteristics of the main roof were not affected by the caving gangue. At the smallest coal seam

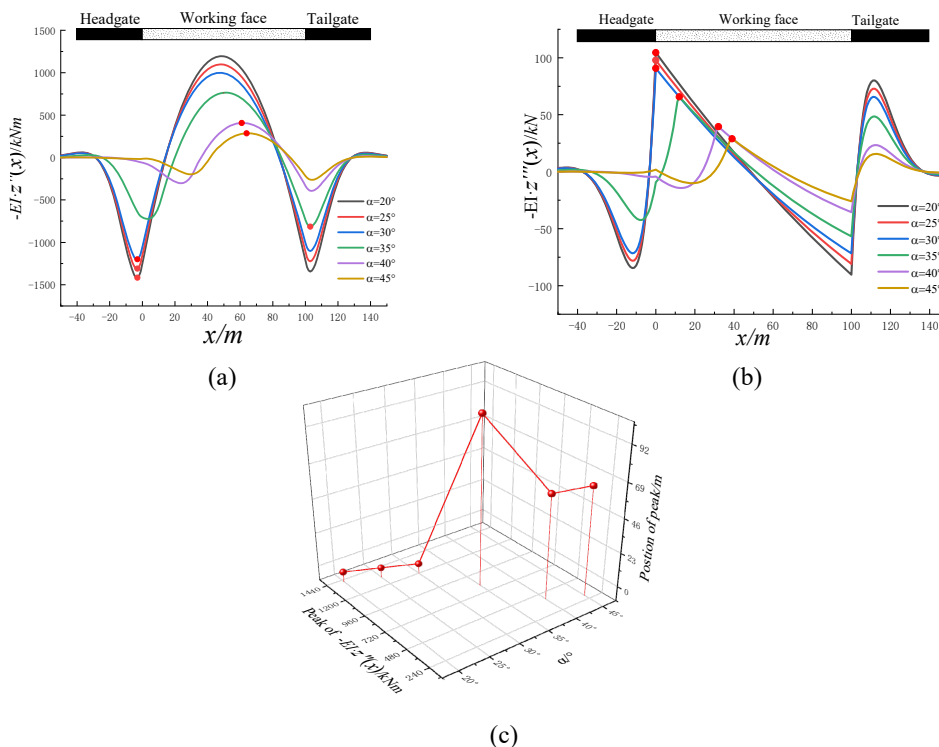


Fig. 11. Bending moment and shear diagram of the rock beam at different angles:
 (a) bending moment, (b) shear, and (c) bending moment varies with angle

angle, the overhang length was at its maximum, and the headgate was damaged first. As the coal seam angle was increased, the normal component for the stress from the self-weight of the rock layer decreased, and the load application point shifted downward. This reduced the bending moment slightly. When the coal seam angle was increased from 20° to 25° and 30° , the bending moment decreased by 7.5% and 15.32%, respectively, and the shear force decreased by 6.37% and 13.12%, respectively.

- (3) When the coal seam angle was greater than the angle of repose of the gangue, increasing the coal seam angle reduced the peak bending moment, and its position migrated from the headgate T-junction to the tailgate T-junction and then the middle of the working face. The peak shear force continuously decreased, and its position was located at the upper end of the contact area. At coal seam angles of 35° , 40° , and 45° , the peak bending moments were -814.04, 408.01, and 285.84 kN-m at positions of 103, 61, and 64 m, respectively. The peak shear forces were 65.58, 39.52, and 28.88 kN at positions of 11.4, 31.58, and 38.37 m, respectively. The accumulation of caving gangue formed a contact area at the lower area of the working face, and increasing the coal seam angle shifted the position of the peak shear force for the lower area of the working face slightly upward. Because the accumulated gangue was much weaker than the rock formation, the peak bending moment was less at the headgate than at the tailgate. When the coal seam angle was further increased, much of the gangue slid or rolled downward, and the lower area of the inclination was filled with caving gangue. The exposed length of the main roof and normal component of the stress from the self-weight of the rock layer continued to decrease. The tensile failure of the main roof occurred first in the middle and upper areas, and the destruction of the roof had a time sequence. Increasing the coal seam angle from 35° to 40° and 45° reduced the bending moment by 49.88% and 64.89%, respectively, and the shear force by 39.73% and 55.96%, respectively.

Therefore, the destruction of the main roof was closely related to the caving effect of the gangue filling at different coal seam angles. As the coal seam angle was increased, more of the gangue filling slid downward, which changed the force and constraint conditions of the main roof in the lower area of the working face. The position where the roof was most easily damaged shifted to the upper area. In this area, the deformation and destruction of the roof were more severe, and the stability of the support was greatly reduced. The support was prone to risks such as unbalanced loading, rotating, and falling. The stability of the support-surrounding rock system for the working face was greatly reduced, so a disaster with the surrounding rock could easily be induced.

7. Field monitoring

7.1. Layout of measurement areas

Working face 25221 of coalmine 2130 was observed for nearly 2 months to understand the interaction between the surrounding rock and supports during the mining process of a steeply dipping coal seam. Fig. 12 shows the three measurement areas along the working face: lower, middle, and upper.

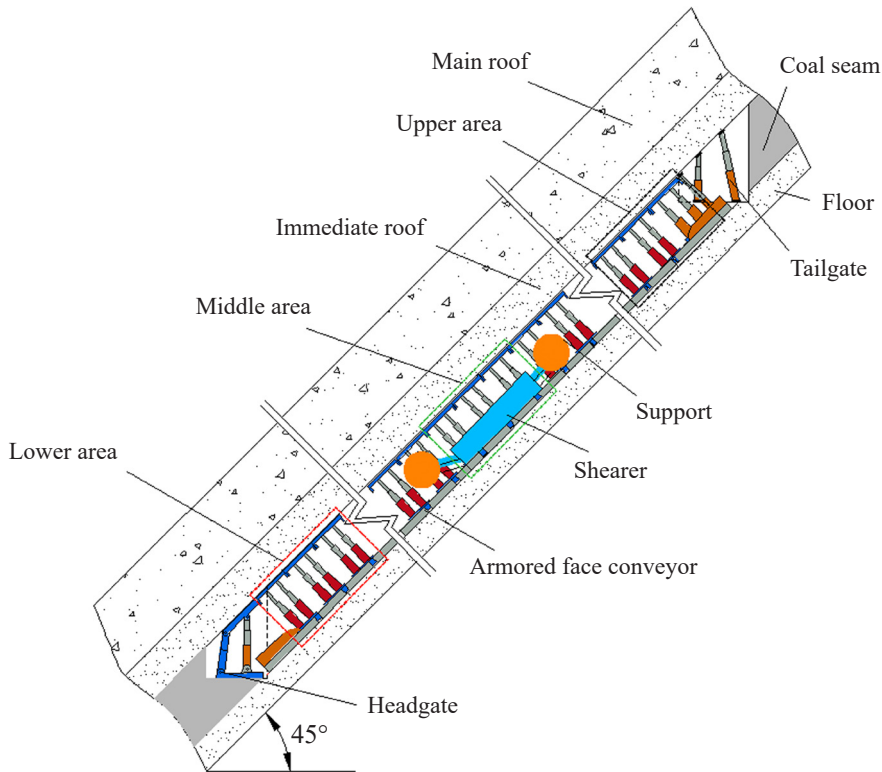


Fig. 12. Arrangement of measurement areas on the working face

7.2. Monitoring method

The KJ377 mining pressure dynamic system was used to observe the mining pressure. The KJ377 pressure monitoring system is carried out by continuously recording the working resistance of the legs of support in the measurement area. The system is mainly composed of ground equipment (server, UPS, serial server) and underground equipment (communication substation, support pressure sensor, etc.). KJ377 can not only realize the computer dynamic simulation display detection parameters and alarms on the ground but also display data and alarms on site. And KJ377 system software can conduct specialized data analysis through mathematical models of rock pressure theory.

The system works as follows. The pressure strain body of the fully mechanized coalmine is connected with the oil-liquid phase of the device through a quick joint. Changes in the roof pressure affect the oil-liquid pressure. The change in the resistance signal generated by the liquid pressure is amplified and transformed by an analog-to-digital converter. The signal is then processed by an 89S52 single chip microcomputer. The current pressure value is displayed on a digital tube, and the data are transmitted to the ground host computer through the monitoring substation. The host computer analyzes the monitoring data to generate historical curves, as shown in Fig. 13.

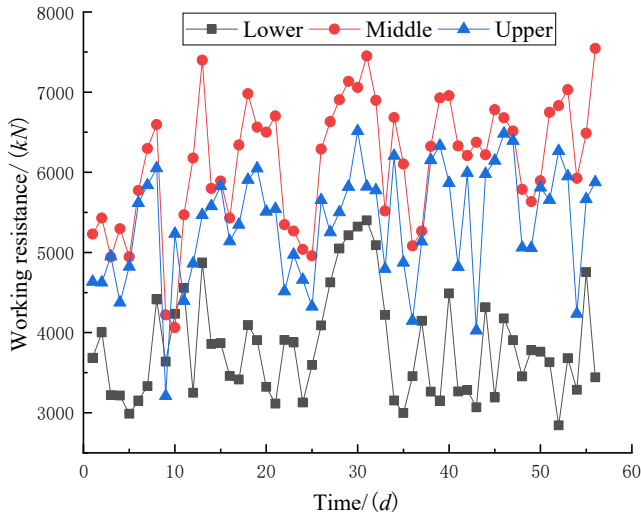


Fig. 13. Loading characteristics of the supports on the working face

7.3. Results and analysis

The field monitoring results were as follows:

- (1) The mining pressure showed obvious localized characteristics along the inclined direction. The average working resistances of the supports in the upper, middle, and lower areas of the working face were about 5370, 6123, and 3815 kN, respectively. The working resistance of the supports indicated a large load in the middle area and smaller loads in the upper and lower areas. The loads on the upper and lower areas were 87.7% and 62.3%, respectively, of the load on the middle area.
- (2) The mean square deviation (standard deviation) was used to analyze the distribution of the working resistance in different areas:

$$s = \sqrt{\frac{\sum_{i=1}^n (x_i - \bar{x})^2}{n}} \tag{36}$$

The mean square deviations of the working resistances of the supports in the upper, middle, and lower areas of the working face were 718.49, 802.1, and 660.92, respectively. Fig. 14 shows the trends for the working resistance distribution of the supports. The working resistance distribution was relatively discrete in the middle and upper areas of the working face, and the distribution was relatively concentrated in the lower area.

- (3) When the strata behavior was considered, the working resistances of the supports in the lower, middle, and upper areas were 5400, 7450, and 6516 kN, respectively. The pressure was high in the middle and upper areas.

When the load and constraints on the roof were unbalanced, there were large differences in the law of load and movement of the supports in different areas along the inclined working

face. In the lower area of the working face, the gangue filling was solid. The migration space, subsidence, and rotation angle of the roof were small, and the support-surrounding rock system was relatively stable. The average working resistance and dispersion of the support were small. In the middle and upper areas of the working face, the gangue filling due to caving was a smaller volume and far from the supports. Thus, the migration space, subsidence, and rotation angle of the roof were greater, and the support-surrounding rock system had poor stability. The contact mode and loading characteristics of the supports and top plate were complex. Phenomena such as partial load, no load, and biting between supports occurred frequently, and the average working resistances of the supports and their dispersion degree were relatively large.

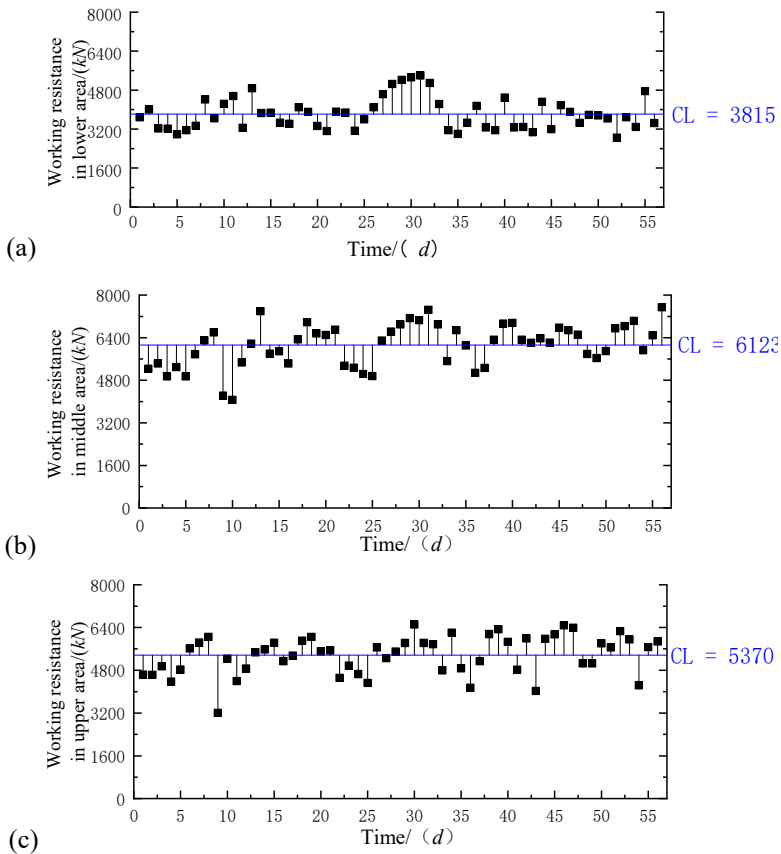


Fig. 14. Quality control chart of the working resistance of supports in the (a) upper, (b) middle, and (c) lower areas

8. Conclusion

Stability control of the roof is the key to safe and efficient mining of the longwall working face for a steeply dipping coal seam. Elastic foundation theory was used to construct a roof

mechanics model, and the effect of the coal seam angle on the asymmetric deformation and failure of the roof was studied under the constraint of unbalanced gangue. The results were as follows:

- (1) The coal seam angle is the main factor that affects the slip characteristics of the gangue filling after caving. The thickness and length of the immediate roof determine the caving volume of the gangue, and the thickness of the coal seam and inclined length of the working face determine the size of the movement space of the gangue. Increasing the coal seam angle, thickness of the immediate roof, and length of the working face and decreasing the thickness of the coal seam increase the length of the contact area formed by the caving gangue in the lower area of the slope. Changes in the length of the contact area affect the force state and boundary conditions of the main roof.
- (2) When the coal seam angle is less than the natural angle of repose of the gangue, changing the former angle only affects the magnitude and acting position of the load on the supports. As the coal seam angle increases, the peak deflection, rotation angle, bending moment, and shear force of the beam decrease. The position of the peak deflection is in the middle area of the working face, and the positions of the peak rotation angle, bending moment, and shear force are in the lower area.
- (3) When the coal seam angle is greater than the natural angle of repose of the gangue, the magnitude and position of the load on the supports will change with the coal seam angle. In addition, the contact area that forms at the lower area affects the stress state and constraints of the main roof. As the coal seam angle increases, the peak deflection, rotation, bending moment, and shear force of the beam decrease sharply. The position of the peak deflection continuously shifts to the upper area of the working face, and the position of the peak rotation shifts from the lower area of the working face to the upper area. The position of the peak bending moment shifts from the headgate T-junction to the tailgate T-junction and then the middle of the working face. The position of the peak shear force is at the upper end of the contact area.
- (4) The asymmetric deformation and failure of the roof led to obvious localized characteristics for the working resistance and degree of dispersion of the supports. In general, the working resistance and degree of dispersion tended to be greatest in the middle area of the working face, followed by the upper area and then the lower area. The slip of the gangue filling in the lower area of the working face gave the roof some stability. The roof frequently failed along the middle and upper areas of the working face; the poor stability of the support-surrounding rock system easily induced failure of the surrounding rock.

These results indicate that a comprehensive monitoring method is required for the mining pressure along the working face of a steeply dipping coal seam. To improve safety, early warning measures are needed to indicate gangue filling part of the middle and upper areas of the working face, frequent roof damage, and changes in the support loading behavior. In the event of a sudden increase in support loads and poor support positions, immediate measures are needed to control the roof and floor of the working face, and the support positions should be adjusted in a timely manner.

Acknowledgment

This work was supported by the National Natural Science Foundation of the PRC (51974227, 51634007) and Major Scientific and Technological Innovation Projects in Shandong Province (2019JZZY020326).

References

- [1] Y.P. Wu, D.F. Yun, P.S. Xie et al., *Progress, practice and scientific issues in steeply dipping coal seams fully-mechanized mining*. J. China Coal Soc. **45** (01):24-34 (2020) (in Chinese).
- [2] Y.P. Wu, B.S. Hu, D. Lang et al., *Risk assessment approach for rockfall hazards in steeply dipping coal seams*. Int. J. Rock Mech. Min. Sci. **138**, 104626 (2021). doi: org/10.1016/j.ijrmms.2021.104626
- [3] D.Y. Zhu, W.L. Gong, Y. Su et al., *Application of High-Strength Lightweight Concrete in Gob-Side Entry Retaining in Inclined Coal Seam*. Advances in Materials Science and Engineering (2020). doi:10.1155/2020/8167038
- [4] H.W. Wang, Y.P. Wu, J.Q. Jiao et al., *Stability Mechanism and Control Technology for Fully Mechanized Caving Mining of Steeply Inclined Extra-Thick Seams with Variable Angles*. Mining, Metall. Explor. (2020). doi:10.1007/s42461-020-00360-0
- [5] R.A. Frumkin, *Predicting rock behaviour in steep seam faces* (in Russian). International Journal of Rock Mechanics and Mining Sciences & Geomechanics Abstracts **20** (1), A12-A13 (1983). doi.org/10.1016/0148-9062(83)91717-5
- [6] A. Ladenko, *Improvements in working steep seams*. International Journal of Rock Mechanics and Mining Sciences & Geomechanics Abstracts **11** (12), 247. (1974). doi.org/10.1016/0148-9062(74)92108-1
- [7] Z. Rak, J. Stasica, Z. Burtan et al., *Technical aspects of mining rate improvement in steeply inclined coal seams: A case study*. Resources **9** (12), 1-16 (2020). doi:10.3390/resources9120138
- [8] H.S. Tu, S.H. Tu, C. Zhang et al., *Characteristics of the Roof Behaviours and mine pressure manifestations during the mining of steep coal seam*. Arch. Min. Sci. **62** (4), 871-890 (2020).
- [9] P.S. Xie, Y.P. Wu, *Deformation and failure mechanisms and support structure technologies for goaf-side entries in steep multiple seam mining disturbances*. Arch. Min. Sci. **64** (3), 561-574 (2019). doi:10.24425/ams.2019.129369
- [10] Z.Y. Wang, L.M. Dou, J. He et al., *Experimental investigation for dynamic instability of coal-rock masses in horizontal section mining of steeply inclined coal seams*. Arabian Journal of Geosciences **13**, 15 (2020). doi:10.1007/s12517-020-05753-5
- [11] P.S. Xie, Y. Luo, Y.P. Wu et al., *Roof Deformation Associated with Mining of Two Panels in Steeply Dipping Coal Seam Using Subsurface Subsidence Prediction Model and Physical Simulation Experiment*. Mining, Metall. Explor. **37** (2), 581-591 (2020). doi:10.1007/s42461-019-00156-x
- [12] X.P. Lai, H. Sun, P.F. Shan et al., *Structure instability forecasting and analysis of giant rock pillars in steeply dipping thick coal seams*. Int. J. Miner. Metall. Mater. **22** (12), 1233-1244 (2015). doi:10.1007/s12613-015-1190-z
- [13] Y.P. Wu, B.S. Hu, P.S. Xie, *A New Experimental System for Quantifying the Multidimensional Loads on an on-Site Hydraulic Support in Steeply Dipping Seam Mining*. Exp. Tech. **43** (5), 571-585 (2019). doi:10.1007/s40799-019-00304-4
- [14] Y.D. Zhang, J.Y. Cheng, X.X. Wang et al., *Thin plate model analysis on roof break of up-dip or down-dip mining slope*. J. Min. Saf. Eng. **27** (4), 487 (2010) (in Chinese).
- [15] J.R. Cao, L.M. Dou, G.A. Zhu et al., *Mechanisms of Rock Burst in Horizontal Section Mining of a Steeply Inclined Extra-Thick Coal Seam and Prevention Technology*. Energies **13** (22), 6043 (2020). doi:10.3390/en13226043
- [16] H.W. Wang, Y.P. Wu, M. Liu et al., *Roof-breaking mechanism and stress-evolution characteristics in partial backfill mining of steeply inclined seams*. Geomatics, Natural Hazards and Risk **11** (1), 2006-2035 (2020). doi:10.1080/19475705.2020.1823491
- [17] S.R. Islavath, D. Deb, H. Kumar, *Numerical analysis of a longwall mining cycle and development of a composite longwall index*. Int. J. Rock Mech. Min. Sci. **89**, 43-54 (2016).
- [18] H. Basarir, O.I. Ferid, O. Aydin, *Prediction of the stresses around main and tail gates during top coal caving by 3D numerical analysis*. Int. J. Rock Mech. Min. Sci. **76**, 88-97 (2015). doi.org/10.1016/j.ijrmms.2015.03.001

- [19] J.A. Wang, J.L. Jiao, *Criteria of support stability in mining of steeply inclined thick coal seam*. Int. J. Rock Mech. Min. Sci. **82**, 22-35 (2016). doi:10.1016/j.ijrmms.2015.11.008
- [20] W.Y. Lv, Y.P. Wu, M. Liu et al., *Migration law of the roof of a composited backfilling longwall face in a steeply dipping coal seam*. Minerals **9** (3) (2019). doi:10.3390/min9030188
- [21] C.F. Huang, Q. Li, S.G. Tian, *Research on prediction of residual deformation in goaf of steeply inclined extra-thick coal seam*. PLoS ONE **15**, 1-14 (2020). doi:10.1371/journal.pone.0240428
- [22] Y.C. Yin, J.C. Zou, Y.B. Zhang et al., *Experimental study of the movement of backfilling gangues for goaf in steeply inclined coal seams*. Arabian Journal of Geosciences **11** (12) (2018). doi:10.1007/s12517-018-3686-0
- [23] G.S.P. Singh, U.K. Singh, *Prediction of caving behavior of strata and optimum rating of hydraulic powered support for longwall workings*. Int. J. Rock Mech. Min. Sci. **47**, 1-16 (2010).
- [24] P.S. Xie, Y.Y. Zhang, S.H. Luo et al., *Instability Mechanism of a Multi-Layer Gangue Roof and Determination of Support Resistance Under Inclination and Gravity*. Mining, Metall. Explor. **37** (5), 1487-1498 (2020). doi:10.1007/s42461-020-00252-3
- [25] G.J. Wu, W.D. Chen, S.P. Jia et al., *Deformation characteristics of a roadway in steeply inclined formations and its improved support*. Int. J. Rock Mech. Min. Sci. **130**, 104324 (2020). doi:10.1016/j.ijrmms.2020.104324
- [26] Y.Q. Long, *Numerical computation of beam on elastic foundation*. People's Education Press, Beijing (1981).